Designing a Distributed Sensing Network for Structural Health Monitoring of Concrete Tunnels

A Case Study

Zhang, Xuehui; Zhu, Hong-Hu ; Jiang, Xi; Broere, Wout; Long, Luyuan

DOI
10.1155/2024/6087901

Publication date
2024

Document Version
Final published version

Published in
Structural Control and Health Monitoring

Citation (APA)
Zhang, X., Zhu, H.-H., Jiang, X., Broere, W., & Long, L. (2024). Designing a Distributed Sensing Network for Structural Health Monitoring of Concrete Tunnels: A Case Study. *Structural Control and Health Monitoring*, *2024*(1), Article 6087901. https://doi.org/10.1155/2024/6087901

Wiley
Structural Control and Health Monitoring
Volume 2024, Article ID 6087901, 17 pages
https://doi.org/10.1155/2024/6087901

WILEY

Research Article

Designing a Distributed Sensing Network for Structural Health Monitoring of Concrete Tunnels: A Case Study

Xuehui Zhang[1,2] **Hong-Hu Zhu**[3] **Xi Jiang**[4] **Wout Broere**[1] **and Luyuan Long**[1]

[1]*Geo-Engineering Section, Department of Geo-Science and Engineering, Delft University of Technology, Delft, Netherlands*
[2]*Department of Civil and Environmental Engineering, The Hong Kong Polytechnic University, Hung Hom, Kowloon, Hong Kong, China*
[3]*School of Earth Sciences and Engineering, Nanjing University, Nanjing 210023, China*
[4]*Department of Geotechnical Engineering, Tongji University, Shanghai 200092, China*

Correspondence should be addressed to Xi Jiang; xi.jiang@polyu.edu.hk and Wout Broere; w.broere@tudelft.nl

Received 28 February 2024; Revised 2 August 2024; Accepted 18 September 2024

Academic Editor: Xiang Shi

Structural health monitoring is essential for the lifecycle maintenance of tunnel infrastructure. Distributed fiber-optic sensor (DFOS) technology, which is capable of distributed strain measurement and long-range sensing, is an ideal nondestructive testing (NDT) approach for monitoring linear infrastructures. This research aims to develop a distributed sensing network utilizing DFOS for structural integrity assessment of concrete immersed tunnels. The primary innovations of this study lie in the development of a general flowchart for establishing a sensing network and obtaining reliable field data, as well as its subsequent validation through a detailed case study. Concentrated joint deformations in typical immersed tunnels, detectable by the DFOS, are key indicators of structural integrity. This study addresses crucial elements of field monitoring system design, including the selection of appropriate optical fibers or cables and the determination of vital interrogator system parameters. It also covers sensor parameter determination, installation techniques, field data collection, and postanalysis. Furthermore, this research is exemplified by a case study that illustrates the successful implementation of a distributed sensing network in an operational immersed tunnel, and monitoring data reveals cyclic structural deformations under impacts of daily tide and seasonal temperature variations. The data obtained from this network play a significant role in subsequent condition assessments of tunnel structures. The research findings contribute to the assessment of large-scale infrastructure health conditions through the application of DFOS monitoring.

Keywords: distributed fiber-optic sensor; immersed tunnel; joint deformation; structural health monitoring; tunnel infrastructure

1. Introduction

Underground tunnel infrastructures have been constructed worldwide, serving vital purposes in human-built environments. Particularly in populated urban areas, a diverse array of tunnels, including those for transportation (roads and railways) and utilities (sewage and drainage), are constructed to expand the use of underground spaces, which substantially contributes to urban sustainability and fortifies resilience against climate change [1–3]. However, as tunnels age, their structural conditions are increasingly compromised by both intrinsic and extrinsic factors, including challenging geological conditions and material degradation [4–6]. For underground tunnels, structural integrity issues are mostly associated with unanticipated excessive deformations, especially at discontinuous points (e.g., construction joints), resulting in leakage and localized concrete cracking [6, 7], thereby emphasizing the importance of preventive monitoring in maintaining the safety and functionality of critical tunnel infrastructures.

Previous studies have investigated various sensing technologies for monitoring tunnel deformations and evaluating their structural integrity. These research efforts encompass health status monitoring from the perspective of construction materials to overall integrity monitoring of large-scale structures. Numerous recent studies have

examined the integration of intelligent technologies into construction materials (primarily concrete and other cementitious composites) to monitor their health conditions and environmental interactions. For instance, Mpalaskas et al. [8] investigated the monitoring of damage propagation and its detection using acoustic emission (AE) techniques, taking into account the scattering of fracture energy within the concrete microstructure. To facilitate intelligent damage detection, small-sized smart piezoelectric sensors have also been successfully deployed in concrete structural members [9–11]. Although these studies are predominantly based on small-scale laboratory tests, they significantly contribute to the development of emerging sensing technologies for structural health monitoring (SHM) from a material perspective.

For monitoring large-scale engineering structures, such as long bridges or tunnels, a variety of potential sensing techniques can be applied for specific purposes. These techniques may include conventional point strain sensors [12], 3D laser scanning [13], computer visions [14], and optical fiber sensor [15]. Among these, distributed fiber-optic sensor (DFOS) stands out for its ability to sense strain, temperature, and vibration over long distances and in a distributed manner. DFOS systems operate on several optical scattering phenomena in light transmission through an optical fiber, including Rayleigh, Brillouin, and Raman scattering [16, 17]. Remarkably, the optical fiber or fiber-optic (FO) cable, potentially extending over a hundred kilometers, functions both as the sensor and the signal transmission medium. This unique feature allows a single cable to serve as a dense array of deformation sensors, covering numerous monitoring points in tunnels [18, 19]. This integrated approach is challenging to replicate with conventional discrete sensors, especially when considering instrumentation costs and the complexity of the sensing network.

In previous studies, DFOS has been used to instrument various geotechnical structures for deformation monitoring [20–24]. For instance, Gue et al. [25] and Zhu et al. [18] used DFOS systems installed on shield tunnels as extensometers on the intrados surface of tunnels to detect transverse torsion and circumferential joint openings. Notably, previous studies have focused mainly on postanalysis of monitoring data, while little emphasis has been placed on the design and establishment of field DFOS monitoring networks. However, if not implemented properly, the DFOS monitoring system may exhibit defects in field conditions, which can deteriorate the measurement accuracy, as evidenced by the work of Zhang and Broere [26] and Liu et al. [27], where issues such as fiber anchorage failure and breakage compromised the performance of the monitoring systems. Particularly under harsh field conditions, a single break can effectively reduce a dual-ended fiber loop to two single-ended fiber lines, which will impact the data acquisition precision, or disable parts of a single-ended monitoring network. Given these challenges, the development of robust field instrumentation guidelines for DFOS monitoring is crucial and should be given as much priority as data interpretation itself.

This study targets to develop a distributed sensing network for monitoring the structural integrity of concrete immersed tunnels using DFOS. The innovations and contributions of the present study are twofold: (1) It proposes a general and practical framework for developing a reliable sensing network and guiding field implementation, and (2) it further verifies the effectiveness of this framework through a tunnel monitoring case study. In the rest of this study, the structural integrity issues of typical immersed tunnels are first discussed in Section 2, and basic monitoring requirements are specified. Subsequently, Section 3 explores the practical design aspects of a distributed monitoring system, and key aspects, such as the criteria for determining sensing fibers or cables and the interrogator system, were initially addressed, followed by critical sensor parameter determination, sensor installation methods, and sensor protection. In addition, the proposed guidelines are explicitly demonstrated through a case study in Section 4, focusing on the successful establishment of a distributed sensing network for monitoring an in-service immersed tunnel. Finally, conclusions of this study are drawn in Section 5.

2. Structural Integrity Issues of Immersed Tunnels

Immersed tunnels, which serve as critical fixed link infrastructures beneath waterways, have been successfully constructed in various locations globally. The construction process typically begins with the fabrication of shorter tunnel segments, which are subsequently assembled into longer elements (typically around 100 m) in a dry dock. These elements are then floated to the designated tunnel site using tugboats and immersed into a prepared trench on the riverbed [28]. Longitudinally, an immersed tunnel structurally behaves akin to a chain of interconnected segments on a prepared foundation. Two distinct types of joints are integral to a segmented immersed tunnel structure, namely, immersion and dilation joints (as depicted in Figure 1). Immersion joints materialize during underwater element immersion and connection, whereas dilation joints form during the sequential fabrication of elements at a dry dock.

Generally, since joint cross sections exhibit a lower bending stiffness than normal cross sections of a continuous structure, making them prone to concentrated excessive deformation. Over an extended operational lifespan, the occurrence of excessive joint deformations predominantly involving longitudinal opening and closure (along y-axis in Figure 1), as well as vertical differential settlements (along z-axis in Figure 1) at the joint, can lead to localized concrete cracking and leakage [6, 29]. Therefore, to comprehensively evaluate structural integrity, it is imperative to diligently monitor joint deformations along the entire length of the tunnel.

3. Monitoring Structure Integrity Using the DFOS

3.1. Basic Information of the DFOS System. A DFOS system generally functions based on optical backscattering phenomena within an optical fiber, encompassing Rayleigh

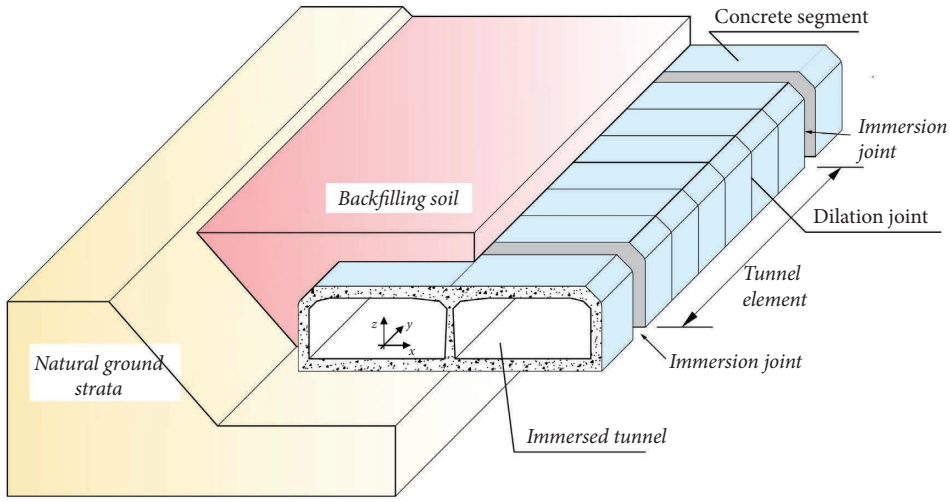

FIGURE 1: Illustration of a segmented immersed tunnel with immersion and dilation joints.

scattering and Brillouin and Raman scattering [16, 17]. DFOS that utilizes Brillouin and Rayleigh backscattering provides distributed strain and temperature sensing capabilities [30], whereas those relying on Raman scattering are limited to temperature measurements. Between the different commercially available Rayleigh scattering–based DFOS systems, optical frequency domain reflectometry (OFDR) is the most suitable given its excellent millimeter-order spatial resolution, but OFDR typically has a sensing range of up to a hundred meters [31], limiting its applicability for monitoring extensive linear infrastructure. In contrast, Brillouin scattering–based DFOS can cover distances up to a hundred kilometers, making them more suitable for monitoring networks in extensive tunnel projects.

3.1.1. Brillouin Scattering–Based DFOS. Brillouin scattering occurs within an optical fiber when forward-propagating incident light interacts with acoustic phonons in optical fibers. This interaction leads to the generation of backscattered light with a shifted frequency compared to the original incident light, which is denoted as the Brillouin frequency shift (BFS), as depicted in Figure 2. The BFS is proportional to the velocity of the acoustic phonons, which is sensitive to mechanical strain or temperature variations in the optical fibers. Therefore, measuring this BFS ($\Delta\nu$) provides a way to determine the strain ε and temperature variations ΔT spatially distributed along the full length of the optical fiber [30, 33]:

$$\Delta\nu = C_\varepsilon \varepsilon + C_t \Delta T, \tag{1}$$

where C_ε and C_t denote the sensitivity coefficients of strain and temperature, respectively, which are typically constant parameters determined by the optical fiber.

3.1.2. DFOS System Parameter Investigation. A typical DFOS setup consists of an optical fiber or cable affixed to the structure and an interrogator device for optical signal analysis (see Figure 2). According to Zhang and Broere [26], when determining a suitable fiber or cable type for extensometer use, the key aspects that should be checked or calibrated include the maximum working strain (MWS), the creep and relaxation potential, the sensitivity coefficients of strain and temperature, and the axial stiffness. Notably, the axial stiffness implies the ease of fiber handling, particularly when prestraining is needed during onsite installation. Conducting a calibration tension test can effectively ascertain the mechanical properties of an optimal sensing fiber, such as by Lienhart et al. [34] and Zhang and Broere [26].

The interrogator performance in DFOS systems is contingent upon several key parameters. The spatial resolution is the primary factor influencing the accuracy of strain or temperature measurements at a given sampling point. This accuracy is derived from averaging over the spatial resolution length, with typical resolutions in civil engineering applications ranging from 2 to 200 cm. Another critical parameter is the maximum sensing distance (MSD), which dictates the maximal length of the optical fiber or cable in DFOS systems. Furthermore, the resolution or accuracy of the BFS is essential. This metric reflects the interrogator's capacity to distinguish the minimum BFS, thus determining the precision of the strain and temperature measurements. Finally, the BFS scan range of an interrogator crucially influences the range of strain and temperature that can be measured. Notably, the practical measurement range in a DFOS system is often more restricted by the properties of the optical fiber itself, especially regarding maximum strain endurance and thermal tolerance. Consequently, when formulating field monitoring strategies, it is imperative to consider both the interrogator capabilities and the intrinsic attributes of the sensing fiber.

3.2. DFOS Instrumentation as Extensometers. As DFOS can measure the strain along the fiber axis, the simplest approach to set up an extensometer is through a two-point anchorage, where a short fiber length is fixed at its two ends, P_1 and P_2, as shown in Figure 3(a). With this layout, the relative displacement of the two anchor points can be readily derived

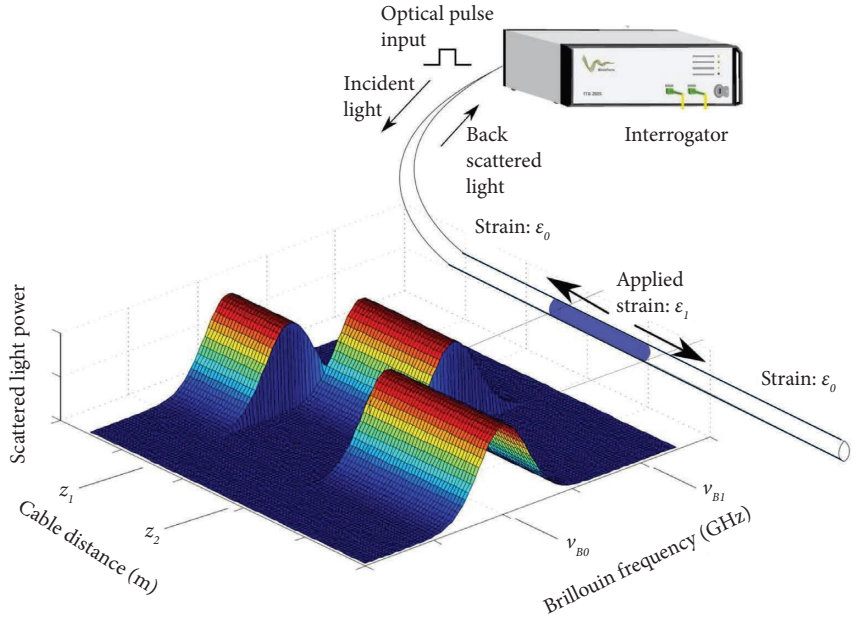

FIGURE 2: Schematic of Brillouin scattering–based DFOS system (modified from [32]).

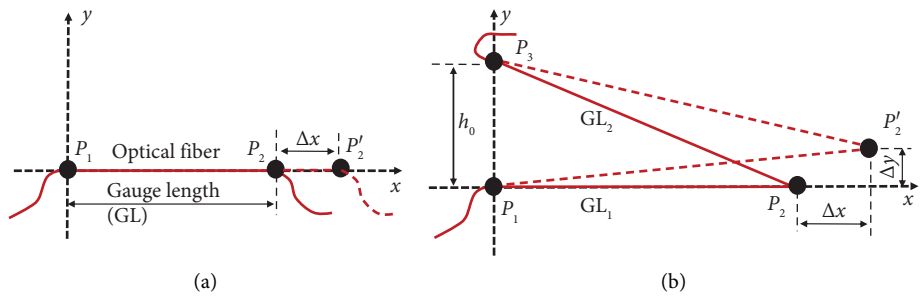

FIGURE 3: Optical fiber extensometer: (a) single form and (b) combined form.

from the extension or contraction of the interval fiber length (Δx in Figure 3(a)). Analogous to the long-gauge fiber Bragg gratings (FBGs) extensometer (for measuring the relative displacement of the two anchor ends), the short interval fiber length is referred to as the gauge length.

Notably, if displacements of P_2 along both the x and y directions (Δx and Δy in Figure 3(b)) are to be measured concurrently, additional extensometers will be required to detect both components precisely, resulting in one possible layout in Figure 3(b), and the mathematical relations correlating fiber strains to displacement components can be derived as follows:

$$\frac{\sqrt{(\mathrm{GL}_1 + \Delta x)^2 + \Delta y^2} - GL_1}{\mathrm{GL}_1} = \varepsilon_1, \tag{2}$$

$$\frac{\sqrt{(\mathrm{GL}_1 + \Delta x)^2 + (h_0 - \Delta y)^2} - \mathrm{GL}_2}{\mathrm{GL}_2} = \varepsilon_2, \tag{3}$$

where GL_1 and GL_2 are the gauge lengths of the two extensometers in Figure 3(b), and h_0 is the vertical distance between the anchor points P_1 and P_3. The fiber strain variations (to the baseline status) of GL_1 and GL_2, namely, ε_1 and ε_2, can be deduced via BFS by the interrogator, and from equations (2) and (3), the accurate displacement components can be derived. The application of such a sensing principle is detailed below in Section 4.2 of case study.

To monitor the concentrated joint deformations of long immersed tunnels, a short length of FO cable can be readily configured as an extensometer spanning the joint gap by fixing its dual ends at two adjoining segments. However, these joint deformations are typically not limited to a single direction but can exhibit more complex deformation modes. First of all, for wide immersed tunnel, the two sidewalls of the joint cross section may settle differently, resulting in segmental twisting (see Δz_1 and Δz_2 in Figure 4(a)), and thus, a proper sensor layout should capture the differential settlements at both sidewalls. Moreover, the thermal expansion or contraction of concrete segments theoretically leads to uniform joint openings, but segment tilting on the vertical plane causes nonuniform opening (variable joint widths) as illustrated in Figure 4(b). These can be monitored using at least two independent extensometers at the upper and lower locations. Given the above monitoring

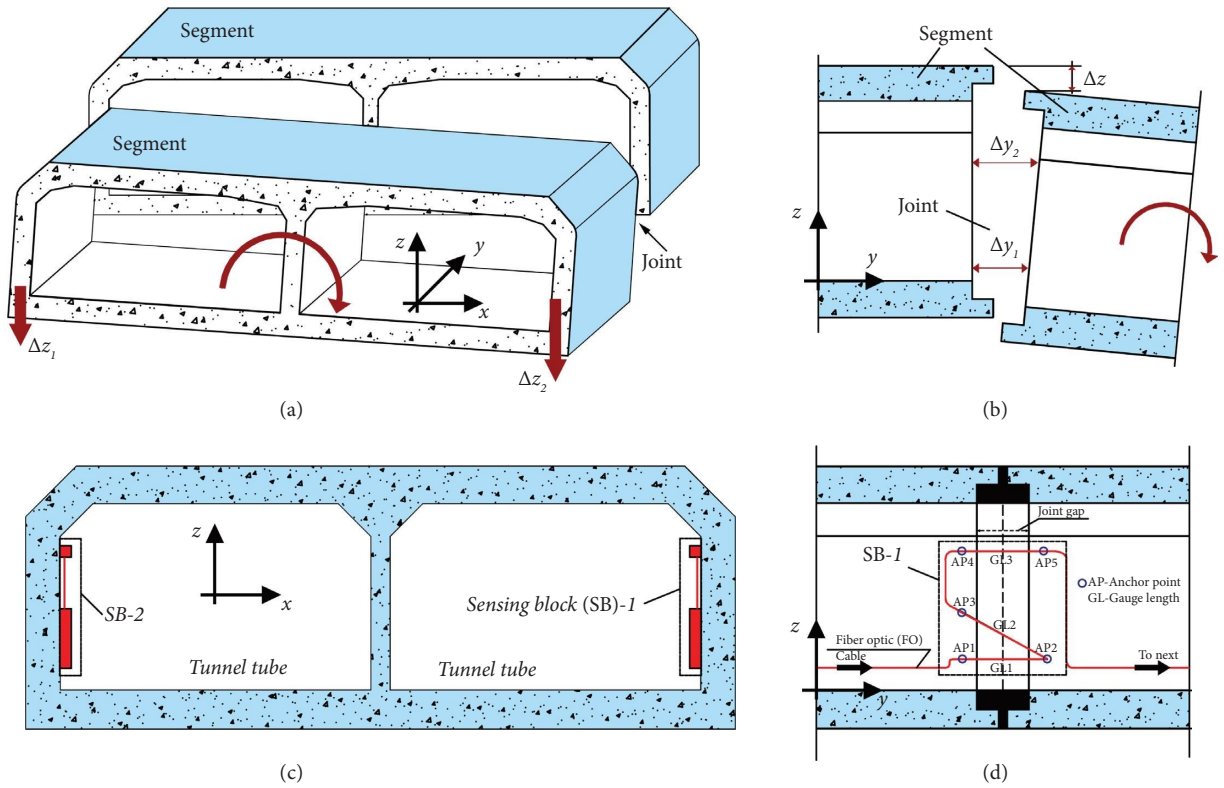

FIGURE 4: Sensor layout at the tunnel joint for measuring deformations: (a) differential settlement transversely; (b) openings and differential settlement at joint; (c) sensor blocks at the tunnel joint; (d) sensor blocks at each sidewall.

requirements, multiple extensometers should be assembled and combined to monitor complex joint deformation modes.

Using DFOS, one feasible instrumentation solution is demonstrated in Figures 4(c) and 4(d). At each joint cross section, two independent sensor blocks (SBs) are installed to instrument both sidewalls. Within each SB, two gauge lengths are horizontally placed (GL1 and GL3 in Figure 4(d)) to detect joint opening at the lower and upper parts of the joint (Δy_1 and Δy_2 in Figure 4(b)). Combined with an additional inclined gauge length GL2, as illustrated in Figure 4(d), the differential settlement at the tunnel joint can be found following the sensing principle proposed in Figure 3(b). Furthermore, the twisting effects resulting from the differential settlements of the two sidewalls (Δz_1 and Δz_2 in Figure 4(a)) can be properly monitored by comparing the vertical settlements of the two SBs. Notably, a single, extended optical fiber has the potential to set up a vast array of measurement points and acquire the needed spatial information for a structural integrity evaluation.

When designing extensometers using optical fibers or cables, the following aspects should be considered.

3.2.1. The Gauge Length. Determining the gauge length is the initial step in extensometer design, and in most cases, the fiber extensometer must be prestrained at installation to be able to measure both elongation and contraction. As illustrated in Figure 5, P_2 defines the gauge length (at zero-strain state), while P_2' indicates the point of installation with an initial prestrain, and P_2'' corresponds to the maximum

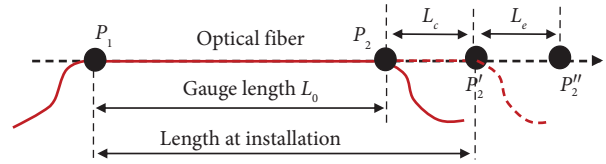

FIGURE 5: Illustration of parameters of a single optical fiber extensometer.

elongation scenario. In order to limit the fiber's working strain below the MWS level at the anticipated maximum displacement (considering both fiber extension and contraction), the gauge length L_0 can be determined as follows:

$$L_0 = (L_c + L_e)\varepsilon_{\max}, \tag{4}$$

where L_c and L_e are the anticipated maximum contraction and elongation (absolute values) of the extensometer, respectively (see Figure 5), and $\varepsilon_{\max}$ is the MWS of the optical fiber.

From the perspective of convenience in extensometer installation, the gauge length should preferably be kept as small as possible; moreover, a shorter gauge length can mitigate the potential vibration of the strained fiber under working conditions. However, the lower bound of the gauge length will still have to take into account that (a) it should preferably be no smaller than the interrogator spatial resolution to minimize the (spatial resolution related) systematic error and (b) the field instrumentation conditions. For instance, the gauge length should be greater than the

joint gap width when installed to span the gap for measuring joint openings.

3.2.2. Fiber Prestrain at Installation. The prestrain level $\varepsilon_{\text{ins.}}$ at installation should account for the maximum contraction scenario as follows:

$$\varepsilon_{\text{ins.}} = \frac{L_c}{L_0}. \tag{5}$$

If L_c and L_e of the extensometer are estimated to be equal, the prestrain level at installation can be set to half of the MWS; hence, the fiber sensing capacity can be fully utilized. Notably, the optical fiber should not be too stiff when manual prestraining is needed during installation.

3.2.3. Compensation of Temperature Effects. As Brillouin scattering depends on temperature and strain, temperature effects must be properly compensated in deformation monitoring. Two common methods are used: measuring the BFS of a short loose (zero-strain) fiber near the gauge length and deducting it from the total BFS, or using a Raman-type distributed temperature sensing (DTS) interrogator for dedicated temperature measurements on the gauge length. The first method is the most widely used for eliminating temperature effects in deformation sensing.

3.2.4. Fiber Anchorage and Protection. For extensometer applications, the gauge length must be securely anchored at both ends to prevent slippage under normal conditions. Directly bonding the fiber to a structure's surface is often impractical due to challenges in prestraining the fiber and the time required for glue to set and harden. Consequently, additional anchoring components, such as anchorage pads or clamps (as depicted in Figure 6), are typically employed. The optical fiber can be affixed to these pads either by gluing onto the surface (see Figure 6(a)), embedding in a glue-filled slot (shown in Figure 6(b)), or using a screw-adjustable clamp (in Figure 6(c)). The (optical fiber-pad) extensometer assembly can then be mounted onto the structure's surface using glue or bolts. Additionally, high strain levels can cause fiber shrinkage and potential slippage at the fiber–clamp or fiber–glue interface, leading to measurement errors. Hence, preinstallation experiments are recommended to test bonding performance with different glues or clamp forces, ensuring reliable anchorage even at the highest anticipated strain levels.

In addition, protecting the extensometer from external impacts is often necessary, particularly for monitoring tasks in harsh environments. Under severe conditions, replacing nonsensing sections with stronger reinforced optical fiber cables by welding connections (ensuring core-cladding layer compatibility) can enhance durability. While such a solution is viable for limited sections due to minor signal loss of approximately 0.1–0.3 dB per connection [25], it also limits the number of reinforced-to-sensing fiber transitions needed to maintain adequate signal quality.

3.3. Workflow for Field Instrumentation Design. In Table 1, a standard workflow is proposed to explicitly demonstrate the procedures for practical field instrumentation design using DFOS extensometers. This workflow covers the essential steps and will be further illustrated with a case study.

The workflow starts by specifying the monitoring requirements or targets as listed in Step 1. The monitoring requirements should cover the directions (single or multiple) and the anticipated range to be measured, the necessity of manual prestrain at installation, and the instrumentation conditions in the field. Note that the field installation conditions further determine the suitable fiber anchorage method. Additionally, if the deformation is to be measured along two or three axes, additional extensometers will be needed, as demonstrated in the case study section.

In Step 2, the collection of key system parameters of the available DFOS system is essential, including the parameters of the optical fiber and interrogator. For a conceptual monitoring system design, the MWS can be set tentatively at 1%, as this applies to most available small-diameter optical fiber products, but further verification is still needed. The spatial resolution of the interrogator can be tentatively set as the lower bound of the extensometer gauge length.

In Step 3, when designing a sensor layout for specific deformation measurements, whether for single- or multi-direction deformations, the relation that transfers the fiber BFS (or fiber strain) to the desired deformations should be established according to specific sensor layouts. Although no universal paradigm exists, this transfer relationship is based on a deformation geometry analysis. A derivation of such a relation is detailed in the case study (Section 4.2).

In Step 4, the gauge length is determined by considering the spatial resolution of the interrogator, the MWS of the optical fiber, and the anticipated deformation range. If fiber prestraining is necessary, the prestrain level should account for the status where the lowest strain scenario occurs on the gauge length. Finally, Step 5 concludes the workflow with the design of the fiber anchorage methods and additional protection measures based on the field working environment.

4. Distributed Monitoring of an Immersed Tunnel Case Study

This section details a case study involving the development and implementation of a DFOS monitoring network for assessing the structural integrity of an immersed tunnel, the Heinenoordtunnel, in the Netherlands. The design of the extensometer and the strategy for field instrumentation are demonstrated through adherence to the workflow outlined in Table 1, validating its applicability.

4.1. First Heinenoordtunnel. The First Heinenoordtunnel, which was opened for service in 1969, is an immersed tunnel located within the A29 highway in the Netherlands that extends beneath the Oude Maas River (see Figure 7). Architecturally, the tunnel features a rectangular cross section and is longitudinally composed of five concrete elements

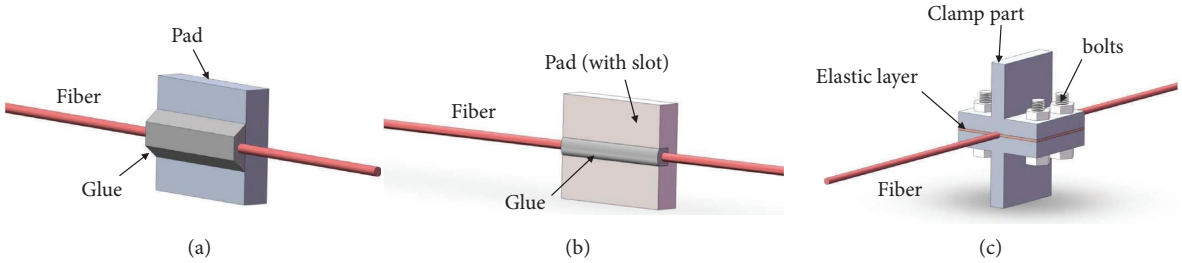

Figure 6: Anchorage pads for fiber fixing: (a) surface bonding; (b) slot bonding; (c) dual clamps (modified from [35]).

Table 1: Workflow of DFOS field instrumentation design.

Work step	Work description
Step 1: monitoring requirements specification	1. Single-direction or multidirection measuring 2. Anticipated range of measured deformation 3. Instrumentation conditions check (mounted on the surface or internal burial) 4. Manual prestrain at installation is needed or not
Step 2: DFOS system parameter collection	1. Spatial resolution of interrogator 2. Maximum working strain of optical fiber (via calibration) 3. Axial stiffness of sensing fiber (if manual prestrain is needed)
Step 3: fiber sensor layout design	1. Establish fiber strain–displacement transfer relation 2. Temperature effects compensation (when needed)
Step 4: gauge length and prestrain	1. Gauge length determination 2. Prestrain level determination
Step 5: fiber anchorage and protection	1. Pad-fiber or clamp-fiber assembly method 2. Field installation planning 3. Fiber protection measures

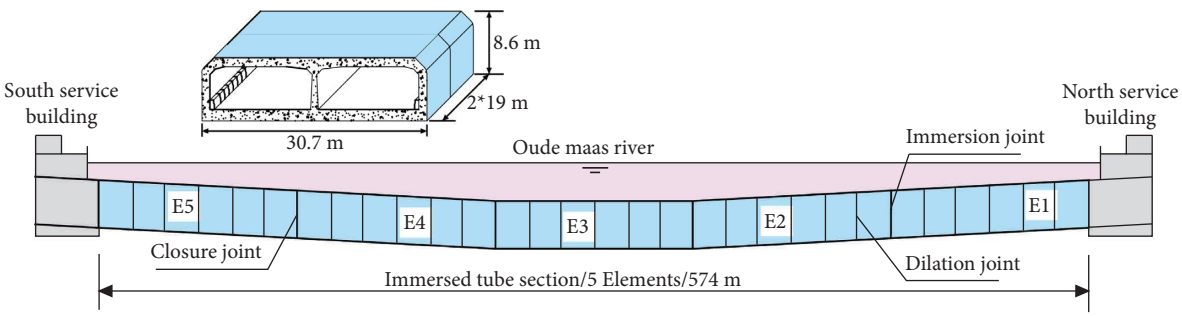

Figure 7: Longitudinal profile of the Heinenoordtunnel.

(labeled E1 to E5 in Figure 7), each extending approximately 115 m in length. These elements are further subdivided into six shorter segments, each measuring approximately 19 m. The total length of this immersed tunnel section is approximately 574 m, incorporating 25 dilation joints and six immersion joints (see Figure 7).

After over 5 decades of operation, the structural integrity concern of the Heinenoordtunnel has increased. Joint leakage has been documented [6, 36] that suggests potential excessive joint opening indicating compromised watertightness [7, 37], while pronounced differential settlements at joints might predict concentrated shear deformation and potential cracking [38]. Consequently, monitoring joint openings and differential settlement is crucial for assessing structural safety throughout a tunnel's service life.

The Heinenoordtunnel is slightly special because, to the extent, there is no central utility tube in the tunnel (as is common for most immersed tunnels), and the only option is to use the main traffic tubes, which results in limited available space for the sensor network configuration, direct exposure of the sensors to traffic, and the added constraint that field installation of the sensors will require temporary tunnel closure to ensure access. The DFOS is chosen for this project because it allows joints to be instrumented with a single optical fiber cable with limited required space (working height from the wall) for individual sensors, and the fiber end can extend outside the tunnel to the end interrogator; hence, a remote-controlled monitoring system that imposes no disturbance on normal traffic becomes possible. The west tube's sidewall in the Heinenoordtunnel is selected for trial sensor instrumentation, as shown in Figure 8.

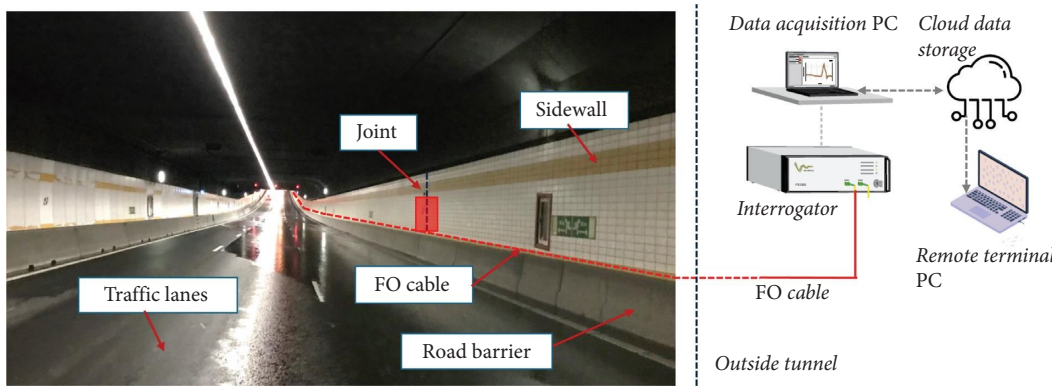

FIGURE 8: Heinenoordtunnel west sidewall to be instrumented by a remotely controllable DFOS system.

4.2. Field Instrumentation Scheme Design. The field instrumentation scheme for the Heinenoordtunnel is designed stepwise as follows.

4.2.1. Step 1: Monitoring Requirement Specification. The target deformations to be monitored are joint deformations along the vertical and longitudinal directions, namely, the joint opening and relative settlement (of the two joint sides), at both the immersion and dilation joints. At immersion joints, an anticipated opening of ±6mm and a relative settlement of approximately ±5mm are expected, and at dilation joints, an anticipated opening of approximately ±4mm and a relative settlement of around ±3mm are expected. Note that a negative opening indicates joint closure relative to the baseline, while a negative differential settlement indicates only an opposite settlement tendency on the two sides compared to the presumed right-handed coordinate system direction. A major constraint is that the installed sensor shall not occupy too much space to limit its potential disturbance to the normal traffic in the tunnel.

4.2.2. Step 2: DFOS System Parameter Collection. In this case study, the determination of the interrogator system includes several project-specific requirements. The commercially available interrogators have been reviewed and discussed by Zhang et al. [15]. Firstly, to cover the tunnel length of approximately 650 m, the interrogator should have a sensing distance exceeding 650 m for single-end measurements or at least 1.3 km for dual-end measurements. Among the available options, Brillouin scattering–based systems are preferred over Rayleigh scattering systems. Secondly, a spatial resolution in the centimeter range is preferable over the meter range, given the need for distributed strain sensing in future applications. Finally, a weighing between cost and performance is necessary.

After a full consideration of the above requirements, a BOFDA interrogator, model fTB2505 produced by fibrisTerre Systems GmbH, was finally selected to measure the BFS in the sensing fibers. This particular BOFDA unit boasts a spatial resolution of 0.2 m for distances up to 2 km and 0.5 m for lengths extending to 25 km. It features a strain accuracy of 2 microstrains (0.0002%) and can measure a maximum strain of 3%, as detailed in FibrisTerre [39].

For extensometer use, a candidate strain-sensing fiber or cable should be checked on several critical metrics, including the MWS, the creep and relaxation potential, and the axial stiffness. Notably, most sensing fiber types in previous studies as evaluated by Zhang et al. [15] can satisfy the MWS requirement. Examples of typical strain-sensing fiber or cables include the D-0.9 mm fiber, the D-2 mm polyurethane-coated FO cable [40], and high-stiffness cables with metal tubes reinforcements, metal reinforcement strings, or glass fiber–reinforced polymer (GFRP) reinforcement [40, 41] as illustrated in Figure 9. In this monitoring project, axial stiffness stands out as a priority since manual prestraining is needed to set up the extensometers. The ultimately selected sensing cable is the polyurethane-sheathed NZS-DSS-C07 type, which features a 2-mm diameter (D-2 mm) as displayed in Figure 9(b). This specific cable exhibited a measured strain sensitivity coefficient of 48.55 MHz per 0.1%, an MWS of approximately 1.2%, and a moderate axial stiffness of approximately 3 kN. These characteristics facilitate relatively easy manual prestraining during installation, as noted by Zhang and Broere [26].

4.2.3. Step 3: Fiber Sensor Layout Design. Due to access limitation, the optical fiber cable is initially planned to be installed only at the west sidewall surface of the tunnel, and at the joint, the cable is aligned as extensometers spanning the joint gap. The SB layout as demonstrated in Figure 4(d) can address the joint deformations of interest, but since the sensor installation is only confined to very short night closures, the extensometer at the upper location will not be implemented. Consequently, this trial monitoring project only targets to monitor the openings and differential settlement at the lower locations of the joints.

For measuring both horizontal and vertical joint deformations simultaneously, two extensometers are set up by fixing the optical fiber at 3 discrete points, P1 to P3, as shown in Figure 10, where both gauge lengths (GL_1 and GL_2) cross the joint gap, and GL_1 works mainly to detect (horizontal) joint openings, while GL_1 and GL_2 strain values can be

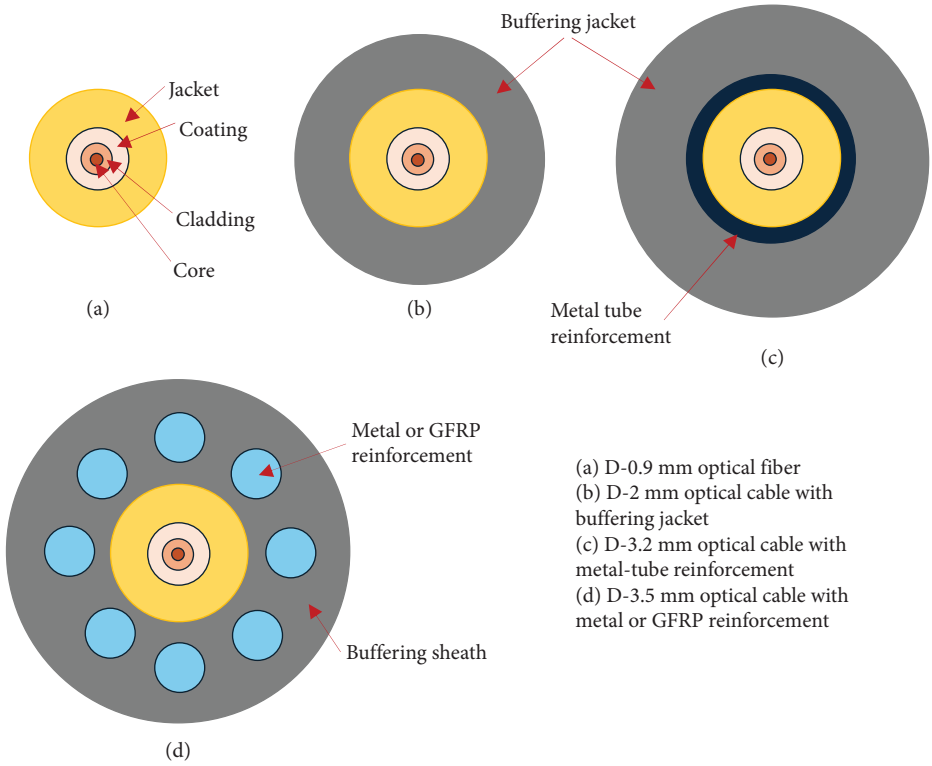

FIGURE 9: Illustration of typical strain-sensing fiber types used in the literature.

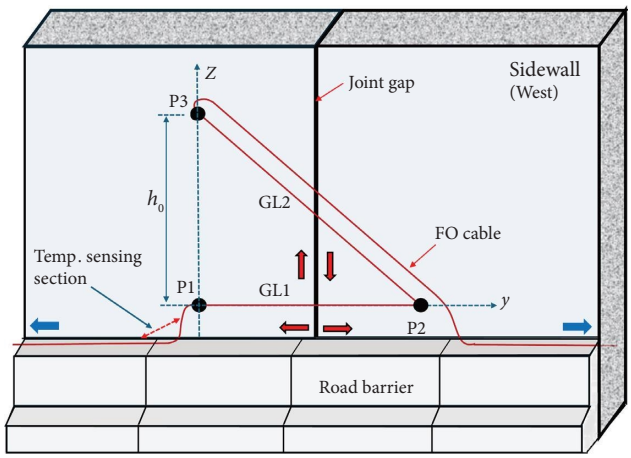

FIGURE 10: Sensor layout for joint two-directional displacement measurements in Heinenoordtunnel.

combined to interpret vertical differential settlement. At installation, GL_1 is set horizontal, and the three fixation points are aligned to form a right-angle triangle. The transfer relations between the measured BFS and joint deformation are derived from geometrical relations, as shown in equations (4)–(9).

Upon the occurrence of a specific joint displacement along both the horizontal and vertical directions at time interval i, the correlation between the fiber's BFS and the deformation for GL_1 can be articulated as follows:

$$\varepsilon_{1,i} = \frac{\Delta\nu_{1,i}}{c_\varepsilon}, \tag{6}$$

$$l_{1.i} = l_1\left(1 + \varepsilon_{1,i}\right), \tag{7}$$

$$\Delta y_i = l_1\varepsilon_{1.i}. \tag{8}$$

For GL_2, it follows that

$$\varepsilon_{2.i} = \frac{\Delta\nu_{2,i}}{c_\varepsilon}, \tag{9}$$

$$l_{2.i} = l_2\left(1 + \varepsilon_{2.i}\right). \tag{10}$$

Moreover, the vertical distance between P1 and P3 is calculated as follows:

$$h_i = \sqrt[2]{l_{2,i}^2 - l_{1,i}^2}. \tag{11}$$

In this context, $l_{1.i}/l_{2.i}$ denotes the length of GL_1/GL_2 at interval i; $\Delta\nu_{1,i}/\Delta\nu_{2,i}$ represents the BFS of GL1 and GL2 at interval i (temperature effects subtracted), as recorded using the interrogator; $\varepsilon_{1.i}/\varepsilon_{2.i}$ are the strains of GL1/GL2; Δy_i is the elongation of GL1 at interval i; and h_i is the vertical distance between the two fixation points P1 and P3.

In the subsequent measurements at a later time interval denoted as j, the relationships between the displacement and BFS, as expressed in equations (6)–(11), still apply. Therefore, the deformation of the joint relative to the previous

interval i can be determined as $(\Delta y_j - \Delta y_i)$ for joint opening and $(h_j - h_i)$ for differential settlement. Note that at immersion and dilation joints, different joint gap widths exist, as shown in Figure 7. However, for simplicity of sensor installation, the sensor layouts at both joints are set the same overall, but with different dimensions and different gauge length values are selected.

At every instrumented joint, the BFS of a short loose fiber length (approximately 40 cm) adjacent to anchor P1 (see Figure 10) within a SB is recorded for the purpose of temperature compensation as well as ambient temperature sensing; in this way, the temperature effects can be deducted (from the total BFS of the tensioned GL_1 and GL_2). The ambient temperature at each joint can be derived from the following equation:

$$T = T_0 + \frac{(f_{t.i} - f_{t.0})}{C_t}, \tag{12}$$

where C_t is the temperature sensitivity coefficient of the optical fiber (1.89 MHz/°C); $f_{t.0}$ indicates the BFS at baseline temperature T_0 (here a room temperature of 22.8°C); and $f_{t.i}$ refers to the BFS at time interval i as recorded by the BOFDA interrogator.

4.2.4. Step 4: Gauge Length and Pretension. The joint gap widths of the immersion and dilation joints are measured to be approximately 135 and 4 cm, respectively. The gauge length determination must consider both the anticipated deformation range and fiber working strains. Here, the MWS of the sensing fiber is set at approximately 1.1%, which is slightly less than the verified MWS of 1.2% to provide additional safety margin. For the immersion joint, the gauge length is determined predominantly by the joint gap width (1.35 m), while for the very narrow dilation joint by the fiber working strain. In addition, the prestraining of fibers at installation should assure strain readings on the two gauge lengths in the extreme scenario where the optical fiber exhibits the loosest status.

The abovementioned conditions result in the governing conditions shown as follows:

$$\frac{2 * \Delta y_{\max}}{L_{1.0}} = \varepsilon_1 \le 1.1\%, \tag{13}$$

$$\frac{\sqrt{\left(L_{1,0} + 2 * \Delta y_{\max}\right)^2 + \left(h_0 + \Delta z_{\max}\right)^2} - L_{2.0}}{L_{2.0}} = \varepsilon_2 \le 1.1\%, \tag{14}$$

$$\frac{\sqrt{{L_{1,0}}^2 + \left(h_0 - \Delta z_{\max}\right)^2} - L_{2.0}}{L_{2.0}} = \varepsilon_2 \ge 0, \tag{15}$$

where $L_{1.0}$ and $L_{2.0}$ indicate the gauge lengths of GL_1 and GL_2, respectively; $\Delta y_{\max}$ and $\Delta z_{\max}$ indicate the anticipated maximum positive opening and differential settlement at the joints, respectively; ε_1 and ε_2 are the strain values of GL_1 and GL_2, respectively; and h_0 is the vertical distance difference between P1 and P3 at the initial installation, as shown in Figure 10, which is set equal to the gauge length of GL_1.

The gauge lengths and prestraining design are determined as listed in Table 2. Note that all the gauge lengths exceed the spatial resolution of the BOFDA (0.2 m), and the corresponding systematic error has been minimized.

4.2.5. Step 5: Fiber Anchorage and Protection. The field installation in the traffic tubes in the Heinenoordtunnel is restricted to several short night closures only; thus, a fast way to set up the SB is essential for working efficiency and project success. Given that pulling the tiny optical fiber to the designated strain level and mounting it directly to the wall surface is inconvenient and can be time-consuming, to quicken the installation process, the fiber is first assembled with anchorage pads using an adhesive at designated positions under laboratory conditions. The pads used are designed with a narrow slot on the surface, where the fiber is embedded by filling with glue, as depicted in Figure 11(b). In the field, the sensors are installed by mounting the pads at the designated locations on the tile surface of the tunnel wall with epoxy adhesive, as shown in Figure 11(a).

As the optical fiber sensors installed are immediately exposed to busy traffic lanes, sensor protection is highly necessary from the start of the monitoring period. Several measures exist that can provide sufficient protection to the sensor: For surface-mounted extensometers, covering the gauge length with plastic or metal cover boards protects against external impacts and isolates the sensors from ambient airflow, which further mitigates fiber vibration; extensometers buried in concrete or ground can be shielded by threading the gauge through a protective tube [27]. Furthermore, the nonsensing sections of the optical fiber serve as signal transmission channels and also require protection, such as by placing them in polyvinyl chloride (PVC) or metal ducts.

Considering the budget and ease of installation, covering protection using thin boards is the optimal solution. In the field, special protective boards that are made of thin stainless steel plates are manufactured to fully cover the SBs at each joint, as shown in Figure 11(c). These boards are installed after the pad mounts and are disconnected at the joint gap to allow for relative deformation. Note that the loose-fiber line GL_3 (see Figure 11(a)) is aligned parallel to GL_2 for ease of covering protection. The finished sensor installation in the Heinenoordtunnel is presented in Figure 12.

In this case, the road barriers on the side of the traffic lanes provide an easy route for the extension of the long FO cable between sensors. These loose cable sections between instrumented joints are encased within a PVC duct for protection, which is mounted atop the road barrier, as shown in Figure 12(b). The field installation procedure is confirmed to be robust enough to be executed even during the peak of the COVID-19 pandemic, despite the resultant delays and restrictions on the number of personnel per night shift. Both ends of the fiber are extended outside the tunnel to the interrogator located within the service room of the

Table 2: Gauge length and pretension design.

Parameter		Immersion joint	Dilation joint
GL1	$L_{1.0}$	1350 mm	800 mm
	Prestraining	0.44% (Installed at 1356 mm)	0.50% (Installed at 804 mm)
	Working strain	0%–0.90%	0%–1.0%
GL2	$L_{2.0}$	1902 mm	1127 mm
	Prestraining	0.60% (Installed at 1913 mm)	0.55% (Installed at 1134 mm)
	Working strain	0.19%–1.01%	0.20%–1.08%

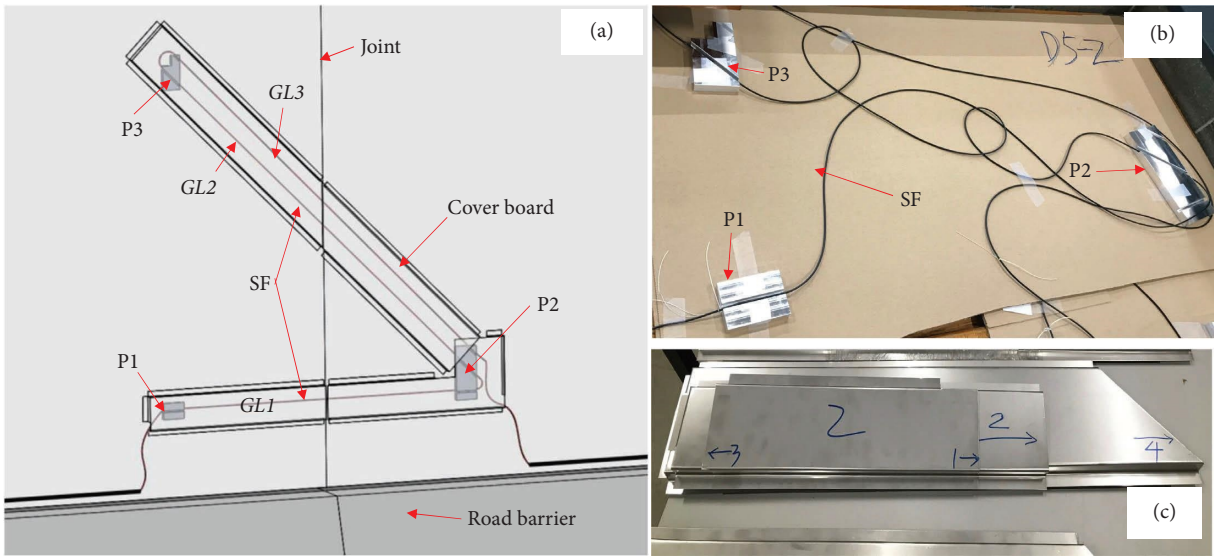

Figure 11: Schematics of the sensor installation scheme in the field: (a) sensor block installation, (b) laboratory fiber-pad assembly, and (c) cover board for fiber sensor protection.

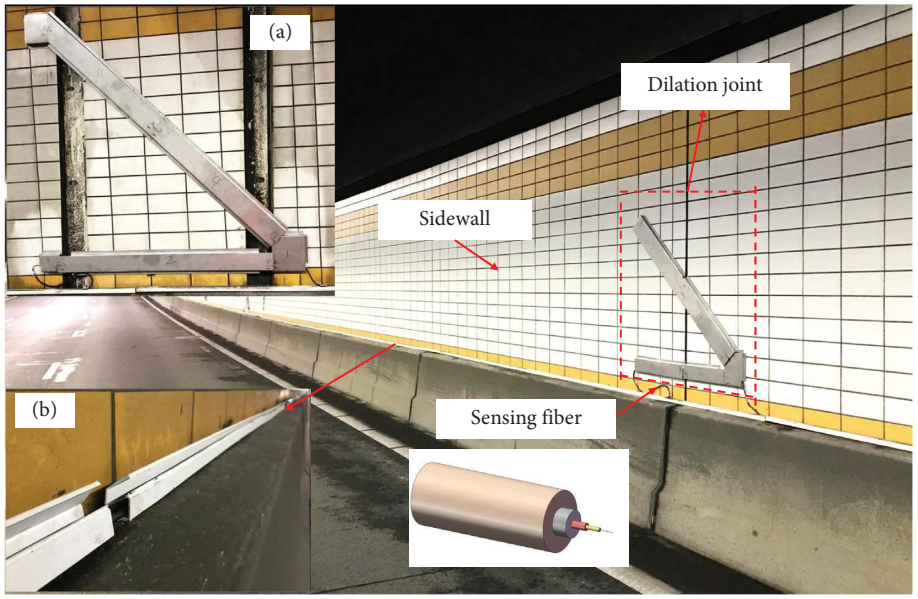

Figure 12: Completed DFOS monitoring network in the First Heinenoordtunnel: (a) sensor block at immersion joints; (b) loose connection FO cable in protective PVC ducts.

tunnel service building above the tunnel entrance. In this way, the installed DFOS monitoring system provides remote controllable ability and imposes no traffic disruptions during operation.

4.3. Monitoring System Performance Appraisal. The DFOS performance of the system installed in the Heinenoordtunnel is assessed with regard to three aspects: the capacity for high-frequency data collection, the signal attenuation level, and the deformation and temperature measurement accuracy.

4.3.1. The Capacity of High-Frequency Data-Taking. The field instrumentation for the complete set of 30 joints (one dilation joint was abandoned due to accessibility limitations) was completed by June 11, 2021. This led to the establishment of a comprehensive optical fiber sensing loop encompassing all the tunnel joints. Under field conditions, one data read for the entire fiber loop took approximately 7 min, demonstrating that the DFOS monitoring system can conduct high-frequency measurements with an interval of less than 1 h. Therefore, it proves capable of performing deformation monitoring for daily and seasonal joint behavior studies of the immersed tunnel.

4.3.2. The Signal Attenuation Level. Signal attenuation of the long optical fiber loop in the field is the key factor determining the precision of BFS measurements. The attenuation of signals within a DFOS system is typically associated with factors such as the length of the fiber, the efficacy of connectors and splices, and the degree of localized bending of the fiber. Under field working conditions, the signal attenuation for the 1.4-km optical fiber loop is measured, using the BOFDA interrogator, as lower than 3.0 dB, which is much smaller than the specified threshold of 12 dB set by the interrogator manual [39]; hence, the BFS measurement results in the field are reliable.

Notably, field observations in this study also reveal that signal attenuation of the optical fiber loop mainly results from severe local fiber bending (beyond the prescribed bending limit), in addition to other factors such as welding connection. In this project, the whole sensing network covering 30 joints, with a length of approximately 1.4 km, was constructed section by section during multiple fieldwork shifts; thus, several welding connections were made, but these connections caused only an insignificant attenuation loss of below 1 dB. However, a deformed cover board due to direct traffic impacts was observed at some points, which caused local bending of the optical fiber and significant signal attenuation of about 12 dB. This local fiber bending only temporarily influenced the system as the high signal deterioration was recovered after cover board maintenance. In conclusion, the installed DFOS system has shown high resilience under field conditions.

4.3.3. Deformation Result Accuracy. A 0.8-m-long reference fiber length was fixed at the tunnel sidewall (not spanning a joint) with an initial strain of around 0.5%. Throughout the 6-month interval spanning from June 12 to December 10, 2021, the strain fluctuation range of this fiber length was approximately 0.01%. Theoretically, this reference fiber length only measures the thermal deformation of the sidewall concrete over a 0.8-m length, which is estimated to be approximately 0.11 mm based on an expansion coefficient of the concrete of 6E − 6 per °C and an average daily temperature difference of 24°C over this period. The deformation measured by the reference fiber length falls in the range of 0.09 mm over the observed period, which agrees with the theoretical value (0.11 mm) on the scale (with the difference far below the desired 0.1-mm accuracy). This finding suggested that the implemented DFOS monitoring network possesses a minimum accuracy of 0.1 mm under field conditions.

4.3.4. Temperature Result Accuracy. To verify the temperature monitoring accuracy, the measured temperature of the most northern joint (the first immersion joint) is compared with the outside meteorological ambient temperature of the site. The results show that temperature measurements by the DFOS system closely follow the ambient weather temperature throughout the monitoring period [42], and therefore, the temperature monitoring results in field conditions are reliable.

In summary, the designed DFOS system in the Heinenoordtunnel proves capable of measuring joint deformation at high frequencies (intervals of less than 1 h) with submillimeter accuracy.

4.4. Monitoring Results Demonstration. To calculate the joint deformations, the BOFDA interrogator first measures the BFS along the fiber cable axis. The BFS readings corresponding to the strained fiber lengths at each individual joint are then obtained. After accounting for the temperature-related BFS, these readings are converted to joint deformations using equations (4)–(9).

4.4.1. Monitoring Results Observation on Daily Basis. Unlike conventional manual leveling with yearly intervals, the DFOS system can record data at minimum intervals of 5 min, effectively revealing joint deformation behavior on a daily basis. The joint deformations and temperature results are presented in Figures 13, 14, 15. It is important to note that the deformations are baselined to June 11, 2021, when monitoring of all 31 joints was initiated.

From the differential settlement results depicted in Figure 13, the most notable behavior is observed in the two troughs at joints J1 and J6. These troughs align closely and recur with a period of approximately 12.5 h. In contrast, the settlement results for the other 28 joints do not exhibit such cyclic behavior to a significant degree. Additionally, joints J1 and J6 are the immersion joints located at the north and south ends of the immersed section, serving as transitions to the piled tunnel abutments. Given the sensor installation at these immersion joints, the regular troughs indicate that the

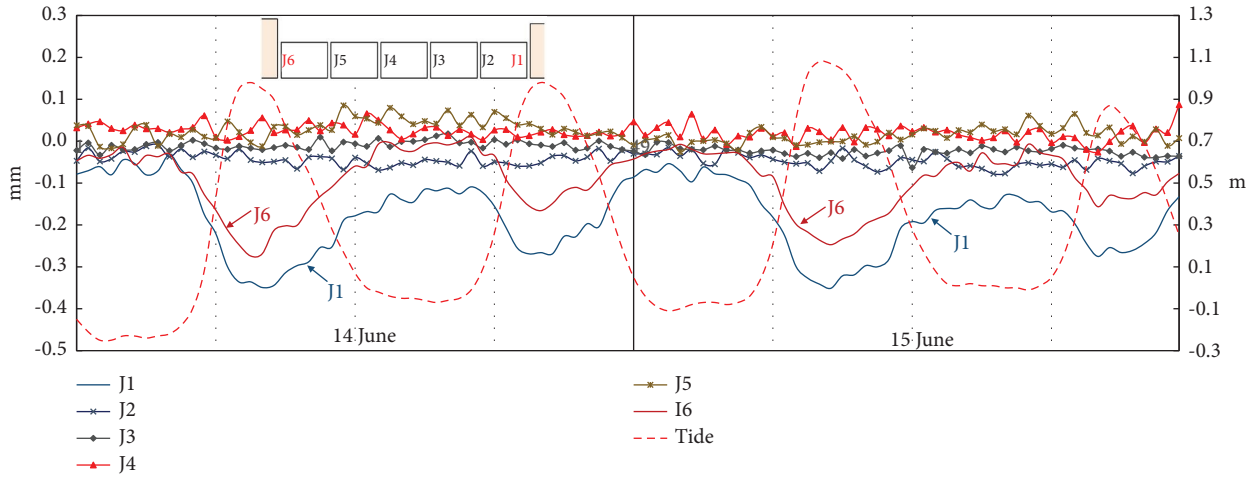

Figure 13: Measured differential settlement at joints (tide level on right vertical axis).

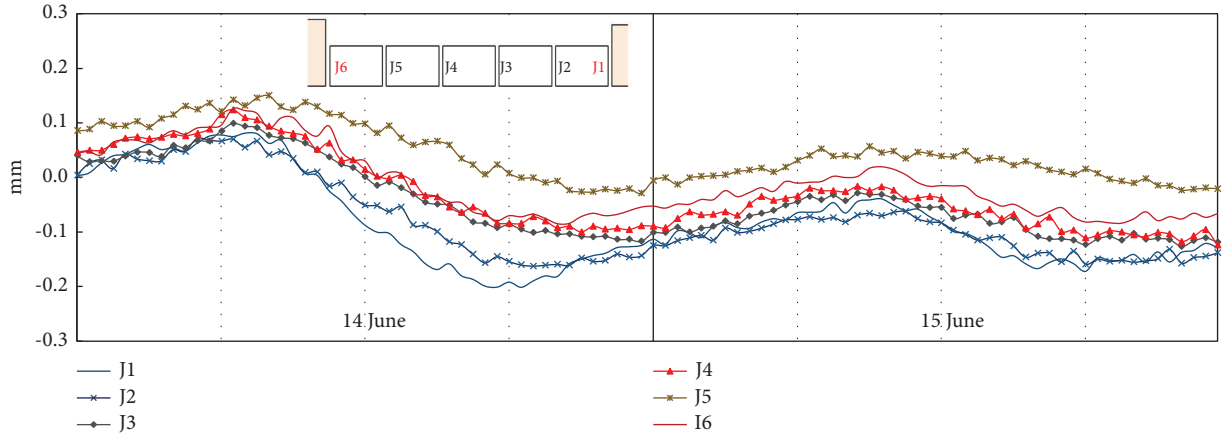

Figure 14: Measured openings results at joints.

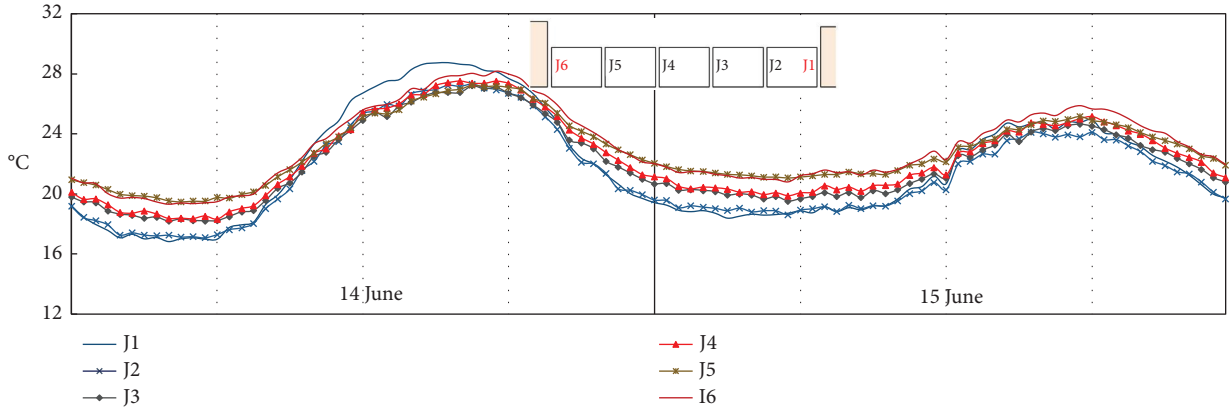

Figure 15: Measured temperature results at joints.

entire immersed tunnel section moves cyclically, almost as a rigid body, relative to the service buildings. The daily cyclic deformation has a roughly 12-h period consistent with the tidal fluctuations in the River Oude Maas at Heinenoord as plotted in Figure 13. This cyclic movement of the tunnel, as detected by the DOFS system, is closely related to the seepage flow and consolidation deformations of the soil strata underlying the tunnel, and for more numerical investigations on this topic, see Zhang and Broere [43].

During this 2-day period, the joint openings range from −0.20 to 0.20 mm. By comparing the data plots in Figures 14 and 15, it is evident that joint opening is generally negatively

correlated with temperature change, where a decrease in temperature corresponds to an increase in joint opening. This suggests that the joint gap tends to open at lower temperatures, such as during winter, and close at higher temperatures, such as during summer. The expectation of seasonal joint opening and closure driven by temperature changes is further validated by the subsequent long-term seasonal deformation results.

4.4.2. Seasonal Tunnel Joint Deformation Behaviors. Field monitoring of the full sensing network, covering all 30 joints, was initiated on June 11, 2021, and concluded on December 11, 2021, due to major tunnel maintenance. The recorded joint deformations of the six immersion joints during this half-year period are presented in Figure 16. The macro deformation results reveal that joint openings are significantly more pronounced than differential settlement. The positive values indicate that, compared to the baseline status on June 11, 2021 (summer), the gaps of all immersion joints widen during winter. However, differential settlement exhibits more significant fluctuations, which are generally less related to seasonal temperature variations.

As a further indication of the seasonal joint deformation behavior revealed by the DFOS monitoring system, Figure 17(a) plots the temperature and joint deformation results (daily mean) of the southernmost immersion joint in the Heinenoordtunnel during the half-year monitoring period (from June 11 to December 10, 2021). During the monitoring period, the absolute joint deformations remained within 1.5 mm, exhibiting seasonal fluctuations with temperature variations. The joint opening exhibited slight fluctuations in the summer season, and as the daily temperature decreased during the winter season, the joint gap widened to a maximum of approximately 1.43 mm by December 10, 2021. Moreover, joint opening has a strong inverse correlation with temperature (with a Pearson correlation coefficient of −0.94), implying that the joint gap expands during the summer and contracts in the winter. The joint differential settlement value (absolute) falls below 0.3 mm, and it also varies with temperature, albeit at a significantly reduced magnitude of fluctuation (evidenced by a Pearson correlation coefficient of 0.31, which is lower than that of joint opening). This suggests a weak correlation between the minor vertical deformations at this joint and temperature. Figure 17(b) plots the results of the second dilation joint in the Heinenoordtunnel during the entire monitoring period (from December 16, 2020, to December 10, 2021). The joint deformations exhibit the same tendency as that of the immersion joint, while the scale of the joint opening (an absolute of 1.5 mm) is much smaller than that of the immersion joint.

Given the thermal properties of concrete, the seasonal variation in joint opening is closely linked to the longitudinal thermal expansion and contraction of the concrete segment. Specifically, during summer, the expansion of the segment leads to a narrowing of the joint gap, resulting in joint closure, whereas in winter, the segment's contraction causes an enlargement of the joint gap, resulting in joint opening. This observation aligns with the hypothesis that the thermal expansion of segments is counterbalanced by cyclic joint opening, as proposed in previous studies [7, 38]. Therefore, the mechanism of seasonal cyclic joint opening at tunnel joints is strongly confirmed by these DFOS measurements. The seasonal joint opening measured by the DFOS system allows for a more explicit analysis of its consequences for joint watertightness and long-term tunnel safety compared with previous studies based only on estimated deformation ranges, as in Van Amsterdam [44] and Van Montfort [38]. In conclusion, the designed DFOS monitoring system demonstrates the capacity to simultaneously detect bi-directional joint deformations (both joint opening and differential settlement) under field conditions, delivering high-quality data. The differential settlement results for the immersion joint fall within the same magnitude as those obtained from previous leveling measurements.

4.5. Discussion and Limitations. Field monitoring has confirmed that the distributed sensing network implemented in the case study can generate joint deformation data at intervals as short as 5 min. This capability allows for the detailed observation of deformation behavior under daily tidal impacts and seasonal temperature variations, which is typically not achievable with conventional leveling methods previously used in monitoring serviced immersed tunnels in the Netherlands. Furthermore, the ability to simultaneously measure horizontal opening and vertical differential settlement of both dilation and immersion joints makes it an ideal monitoring solution for assessing the structural integrity of long immersed tunnels. The cover boards provide sufficient protection to the sensing fiber, although a traffic accident caused an impact to the sensing fiber resulting in significant signal loss, which was subsequently recovered during site maintenance. Overall, the DFOS monitoring network has proven highly effective in upgrading the current monitoring of immersed tunnel infrastructures.

However, there exist limitations in this study. Regrettably, due to accessibility limitations, no other reference instruments were installed to provide explicit joint opening measurements comparable to those acquired by the DFOS system. In this trial monitoring study, the DFOS network was installed only on the lower section of one sidewall. The proposed ideal sensor layout depicted in Figure 4, which includes measurements of segment tilting and skewing, could not be fully implemented due to site accessibility limitations in the Heinenoordtunnel. However, such a comprehensive sensor layout is planned for future monitoring practices, following the completion of the ongoing major tunnel renovation that includes the construction of a narrow utility tube for improved accessibility. The DFOS is planned to be installed at additional locations on the tunnel structure to better characterize spatial deformation behaviors, in combination with other comparable sensor types for validation. Following the validated performance in the trial monitoring, the DFOS will be further extended to upgrade large-scale tunnel infrastructure monitoring in the Netherlands during the next-stage maintenance campaign.

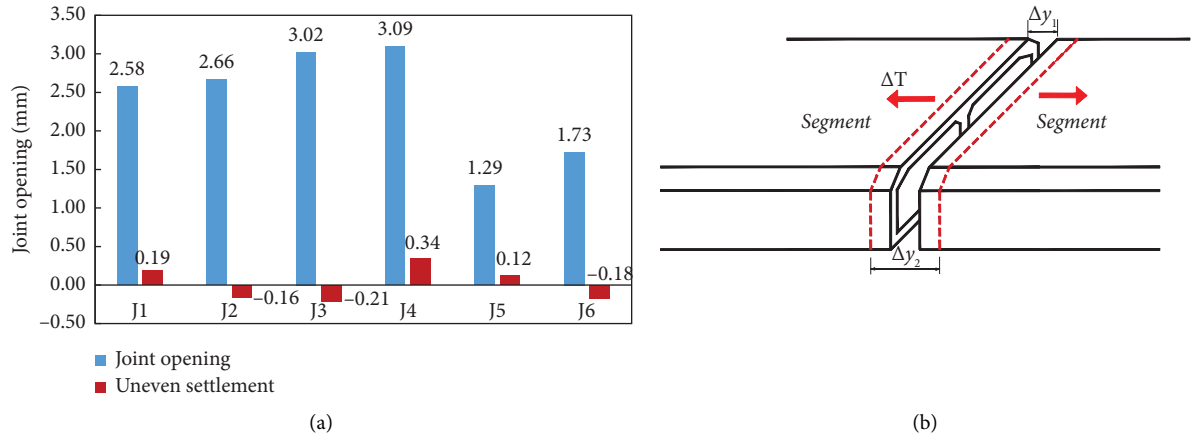

FIGURE 16: The joint deformations of immersion joints: (a) deformation ranges and (b) joint opening behavior due to seasonal segment thermal deformation.

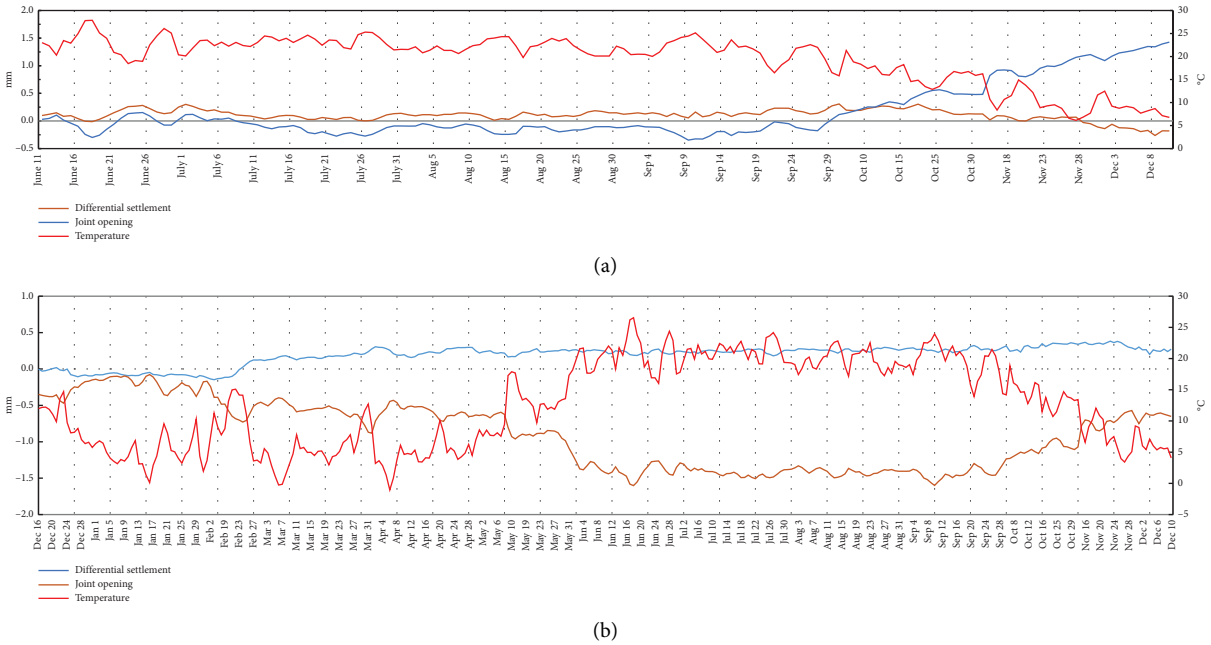

FIGURE 17: Monitored deformations of the (a) most southern immersion joint and (b) the second southernmost dilation joint (temperature results on right vertical axis).

5. Conclusion

DFOS offers a solution to the limitations of traditional sensor types, providing extensive spatial and temporal data crucial for structural condition assessments. This research focuses on developing a DFOS-based distributed sensing network for evaluating the structural integrity of concrete immersed tunnels. A case study from the Netherlands exemplifies the feasibility of the approach. General conclusions include the following:

1. In developing a DFOS-based distributed sensing network for structural monitoring, the overall system performance under field conditions hinges on the properties of the optical fiber, the capabilities of the interrogator system, and the quality of the field sensor installation.
2. The installation of DFOS as extensometers for monitoring concentrated deformation involves considerations such as gauge length determination, prestrain at installation, temperature effect compensation, fiber anchorage, and protection.
3. The practical workflow proposed for designing and implementing DFOS instrumentation under field conditions has been proven effective through the case study. The deployed DFOS system demonstrated the capability to measure bidirectional joint deformations (joint opening and differential settlement) at subhour intervals, confirming its validity in site conditions.

4. The distributed sensing network in the case study effectively quantifies the cyclic opening and closure of joints driven by temperature variations in the immersed tunnel. Monitoring over both daily and seasonal periods indicates that the joint gap tends to open at lower average temperatures and close at higher temperatures.
5. High-frequency monitoring data reveal that the entire immersed tunnel section behaves like a rigid body, moving upward and downward periodically with tidal variations, with a submillimeter movement amplitude. Consequently, the DFOS sensing network enhances the SHM of immersed tunnels and provides more comprehensive information for assessing their long-term integrity and safety.

In summary, the proposed framework for creating the sensing network and acquiring reliable field data, along with its verification through a case study, potentially enhances the application of DFOS for tunnel infrastructure monitoring and assessment within maintenance campaigns. However, this study has limitations, as it does not achieve a fully comprehensive sensing network capable of capturing the spatial deformation behaviors of the structure, nor does it delve into structural health assessment based on the monitoring data. These are crucial aspects that warrant further investigation in subsequent studies.

Data Availability Statement

The authors confirm that the data supporting the findings of this study are available within the article.

Conflicts of Interest

The authors declare no conflicts of interest.

Funding

This research was financially supported by Rijkswaterstaat, the Netherlands, the European Union's Horizon 2020 Project SAFE-10-T, and the China Scholar Council (China).

Acknowledgments

This research was financially supported by Rijkswaterstaat, the Netherlands, the European Union's Horizon 2020 Project Safe-10-T, and the China Scholar Council (China).

References

[1] W. Broere, "Urban Underground Space: Solving the Problems of Today's Cities," *Tunnelling and Underground Space Technology* 55 (2016): 245–248, https://doi.org/10.1016/j.tust.2015.11.012.

[2] D. Xu, X. Zhang, W. Chen, X. Jiang, Z. Liu, and Y. Bai, "Utilisation of the Deep Underground Space in Shanghai," *Proceedings of the Institution of Civil Engineers-Municipal Engineer* 172, no. 4 (2019): 218–223, https://doi.org/10.1680/jmuen.18.00029.

[3] J. Cui, W. Broere, and D. Lin, "Underground Space Utilisation for Urban Renewal," *Tunnelling and Underground Space Technology* 108 (2021): https://doi.org/10.1016/j.tust.2020.103726.

[4] Y. Yuan, Y. Bai, and J. Liu, "Assessment Service State of Tunnel Structure," *Tunnelling and Underground Space Technology* 27, no. 1 (2012): 72–85, https://doi.org/10.1016/j.tust.2011.07.002.

[5] V. Di Murro and L. Pelecanos, "Long-Term Deformation Monitoring of CERN Concrete-Lined Tunnels Using Distributed Fibre-Optic Sensing," *Geotechnical Engineering Journal of the SEAGS and AGSSEA* 50, no. 2 (2019): 1–7.

[6] K. G. Gavin, W. Broere, M. S. Kovačević, and K. de Haas, "Investigation of the Remaining Life of an Immersed Tube Tunnel," in *Tunnels and Underground Cities. Engineering and Innovation Meet Archaeology, Architecture and Art* (Boca Raton, FL: CRC Press, 2019), 4831.

[7] Y. Bai and H. Lu, "Damage Analysis and Repair Technology of OMEGA Gasket in Immersed Tube Tunnel," *Journal of Railway Engineering Society* 9 (2016): 87–92.

[8] A. C. Mpalaskas, T. E. Matikas, and D. G. Aggelis, "Acoustic Monitoring for the Evaluation of Concrete Structures and Materials," in *Acoustic Emission and Related Non-destructive Evaluation Techniques in the Fracture Mechanics of Concrete* (Sawston, UK: Woodhead Publishing, 2021), 257–280, https://doi.org/10.1016/B978-0-12-822136-5.00013-7.

[9] C. G. Karayannis, E. Golias, M. C. Naoum, and C. E. Chalioris, "Efficacy and Damage Diagnosis of Reinforced Concrete Columns and Joints Strengthened With FRP Ropes Using Piezoelectric Transducers," *Sensors* 22, no. 21 (2022): 8294, https://doi.org/10.3390/s22218294.

[10] D. Ai, D. Zhang, and H. Zhu, "Damage Localization on Reinforced Concrete Slab Structure Using Electromechanical Impedance Technique and Probability-Weighted Imaging Algorithm," *Construction and Building Materials* 424 (2024): https://doi.org/10.1016/j.conbuildmat.2024.135824.

[11] N. A. Papadopoulos, M. C. Naoum, G. M. Sapidis, and C. E. Chalioris, "Resilient and Sustainable Structures Through EMI-Based SHM Evaluation of an Innovative C-FRP Rope Strengthening Technique," *Applied Mechanics* 5, no. 3 (2024): 405–419, https://doi.org/10.3390/applmech5030024.

[12] F. Rauch and O. Fischer, "Structural Monitoring of Segmental Tunnel Linings: Toward Safer and More Resource-Efficient Tunnels," *Civil Engineering Design* 4, no. 1-3 (2022): p62–p71, https://doi.org/10.1002/cend.202100053.

[13] S. Kalenjuk and W. Lienhart, "Drive-by Infrastructure Monitoring: A Workflow for Rigorous Deformation Analysis of Mobile Laser Scanning Data," *Structural Health Monitoring* 23, no. 1 (2024): 94–120, https://doi.org/10.1177/14759217231168997.

[14] S. Hou, Z. Ou, Y. Huang, and Y. Liu, "Pixel-Level Crack Segmentation of Tunnel Lining Segments Based on an Encoder–Decoder Network," *Frontiers of Structural and Civil Engineering* 18, no. 5 (2024): 681–698, https://doi.org/10.1007/s11709-024-1048-4.

[15] X. Zhang, H. Zhu, X. Jiang, and W. Broere, "Distributed Fiber Optic Sensors for Tunnel Monitoring: A State-of-the-Art Review," *Journal of Rock Mechanics and Geotechnical Engineering* 16, no. 9 (2024): 3841–3863, https://doi.org/10.1016/j.jrmge.2024.01.008.

[16] J. M. López-Higuera, L. Rodriguez Cobo, A. Quintela Incera, and A. Cobo, "Fiber Optic Sensors in Structural Health Monitoring," *Journal of Lightwave Technology* 29, no. 4 (2011): 587–608, https://doi.org/10.1109/JLT.2011.2106479.

[17] A. Hartog, *An Introduction to Distributed Optical Fiber Sensors* (Boca Raton, FL: CRC Press, Taylor & Francis Group, 2017).

[18] H. H. Zhu, D. Y. Wang, B. Shi, X. Wang, and G. Q. Wei, "Performance Monitoring of a Curved Shield Tunnel During Adjacent Excavations Using a Fiber Optic Nervous Sensing System," *Tunnelling and Underground Space Technology* 124 (2022): https://doi.org/10.1016/j.tust.2022.104483.

[19] D. Wang, H.-H. Zhu, J. Huang, Z. Yan, X. Zheng, and B. Shi, "Fiber Optic Sensing and Performance Evaluation of a Water Conveyance Tunnel With Composite Linings Under Super-High Internal Pressures," *Journal of Rock Mechanics and Geotechnical Engineering* 15, no. 8 (2023): 1997–2012, https://doi.org/10.1016/j.jrmge.2023.02.026.

[20] A. Klar and R. Linker, "Feasibility Study of Automated Detection of Tunnel Excavation by Brillouin Optical Time Domain Reflectometry," *Tunnelling and Underground Space Technology* 25, no. 5 (2010): 575–586, https://doi.org/10.1016/j.tust.2010.04.003.

[21] X. Wang, B. Shi, G. Wei, S. E. Chen, H. Zhu, and T. Wang, "Monitoring the Behavior of Segment Joints in a Shield Tunnel Using Distributed Fiber Optic Sensors," *Structural Control and Health Monitoring* 25, no. 1 (2018): e2056, https://doi.org/10.1002/stc.2056.

[22] H. J. Li, H. H. Zhu, H. Y. Wu, B. Zhu, and B. Shi, "Experimental Investigation on Pipe-Soil Interaction Due to Ground Subsidence via High-Resolution Fiber Optic Sensing," *Tunnelling and Underground Space Technology* 127 (2022): https://doi.org/10.1016/j.tust.2022.104586.

[23] S. Zhao, D. Tan, S. Lin, Z. Yin, and J. Yin, "A Deep Learning-Based Approach With Anti-Noise Ability for Identification of Rock Microcracks Using Distributed Fibre Optic Sensing Data," *International Journal of Rock Mechanics and Mining Sciences* 170 (2023): https://doi.org/10.1016/j.ijrmms.2023.105525.

[24] S. Q. Lin, D. Tan, Y. F. Leung, et al., "Fiber-Optic Monitoring of a Twin Circular Shaft Excavation: Development of Circumferential Forces and Bending Moments in Diaphragm Walls," *Journal of Geotechnical and Geoenvironmental Engineering* 149, no. 12 (2023): https://doi.org/10.1061/jggefk.gteng-11211.

[25] C. Y. Gue, M. Wilcock, M. M. Alhaddad, M. Z. E. B. Elshafie, K. Soga, and R. J. Mair, "The Monitoring of an Existing Cast Iron Tunnel With Distributed Fibre Optic Sensing (DFOS)," *Journal of Civil Structural Health Monitoring* 5 (2015): 573–586, https://doi.org/10.1007/s13349-015-0109-8.

[26] X. Zhang and W. Broere, "Sensing Fiber Selection for Point Displacement Measuring With Distributed Optic Fiber Sensor," *Measurement* 197 (2022): https://doi.org/10.1016/j.measurement.2022.111275.

[27] W. Liu, H. Zhou, B Wang, et al., "A Subgrade Cracking Monitoring Sensor Based on Optical Fiber Sensing Technique," *Structural Control and Health Monitoring* 25, no. 9 (2018): e2213, https://doi.org/10.1002/stc.2213.

[28] R. Lunniss and J. Baber, *Immersed Tunnels* (Boca Raton, FL: CRC Press, 2013).

[29] S. Wang, X. Zhang, and Y. Bai, "Comparative Study on Foundation Treatment Methods of Immersed Tunnels in China," *Frontiers of Structural and Civil Engineering* 14, no. 1 (2020): 82–93, https://doi.org/10.1007/s11709-019-0575-x.

[30] A. Motil, A. Bergman, and M. Tur, "State of the Art of Brillouin Fiber-Optic Distributed Sensing," *Optics and Laser Technology* 78 (2016): 81–103, https://doi.org/10.1016/j.optlastec.2015.09.013.

[31] L. Palmieri, L. Schenato, M. Santagiustina, and A. Galtarossa, "Rayleigh-Based Distributed Optical Fiber Sensing," *Sensors* 22, no. 18 (2022): 6811, https://doi.org/10.3390/s22186811.

[32] L. Pelecanos, K. Soga, M. Z. E. B. Elshafie, et al., "Distributed Fiber Optic Sensing of Axially Loaded Bored Piles," *Journal of Geotechnical and Geoenvironmental Engineering* 144, no. 3 (2018): https://doi.org/10.1061/(asce)gt.1943-5606.0001843.

[33] H. Ohno, H. Naruse, M. Kihara, and A. Shimada, "Industrial Applications of the BOTDR Optical Fiber Strain Sensor," *Optical Fiber Technology* 7, no. 1 (2001): 45–64, https://doi.org/10.1006/ofte.2000.0344.

[34] W. Lienhart, F. Moser, H. Schuller, and T. Schachinger, "Reinforced Earth Structures at Semmering Base Tunnel-Construction and Monitoring Using Fiber Optic Strain Measurements," in *Proceedings of the 10th International Conference on Geosynthetics (10ICG)* (Berlin, Germany, July 2014).

[35] M. Iten and Hauswirth, "Distributed Fiber Optic Sensor Development, Testing, and Evaluation for Geotechnical Monitoring Applications," in *SPIE Smart Structures and Materials + Nondestructive Evaluation and Health Monitoring* (San Diego, CA, USA, 2011).

[36] Rijkswaterstaat Gpo, "Report-Deformatiemeting-37H-312-01," (2016), https://scholar.google.com/scholar?q=Rijkswaterstaat%20GPO._2016._Report-Deformatiemeting-37H-312-01.

[37] R. Rahadian, S. van der Woude, D. Wilschut, C. B. Blom, and W. Broere, "A New Test Setup for Studying Sand Behaviour Inside an Immersed Tunnel Joint Gap," in *Physical Modelling in Geotechnics* (Boca Raton, FL: CRC Press, 2018), 443–448.

[38] R. Van Montfort, "Insufficiency of Immersion Joints in Existing Immersed Tunnels: Case Study on Functioning of Gina-Seal and Omega-Seal in the Kil Tunnel" (MSc Thesis, Delft, Netherlands: Delft University of Technology, 2018).

[39] Fibristerre, "Information of BOFDA Interrogator See," (2021), https://www.fibristerre.de/files/BOFDA_distributed_fiber-optic_sensing.pdf.

[40] Nanzee Sensing, "Optical Fiber Cable Products Information," (2022), https://www.nzsensing.com/cpzx/info_3.aspx?itemid=475.

[41] Solifos Ag, "BRUsens DSS V3 and V9 Strain Cable Information," (2023), https://solifos.com/en/sensing/structural-health-monitoring.

[42] X. Zhang and W. Broere, "Monitoring Seasonal Deformation Behavior of an Immersed Tunnel With Distributed Optical Fiber Sensors," *Measurement* 219 (2023): https://doi.org/10.1016/j.measurement.2023.113268.

[43] X. Zhang and W. Broere, "Monitoring of Tidal Variation and Temperature Change-Induced Movements of an Immersed Tunnel Using Distributed Optical Fiber Sensors (DOFSs)," *Structural Control and Health Monitoring* 2023 (2023): 2419495, https://doi.org/10.1155/2023/2419495.

[44] B. Van Amsterdam, "Probabilistic Analysis of Immersed Tunnel Settlement Using CPT and MASW" (MSc Thesis, Delft, Netherlands: Delft University of Technology, 2019).